

# Rotating BHs as Central Engines of Long GRBs: Faster is Better

Shigehiro NAGATAKI

*Yukawa Institute for Theoretical Physics, Kyoto University, Oiwake-cho Kitashirakawa Sakyo-ku, Kyoto 606-8502, Japan  
nagataki@yukawa.kyoto-u.ac.jp*

(Received ; accepted )

## Abstract

We performed simulations of collapsars with different Kerr parameters  $a=0, 0.5, 0.9, 0.95$ . It is shown that a more rapidly rotating black hole is driving a more energetic jet. No jet is seen for the case of Schwarzschild black hole case, while the total energy of the jet is as large as  $10^{50}$  erg for a rapidly rotating Kerr black hole case ( $a=0.95$ ). In order to explain the high luminosity of a GRB, it is concluded that a rapidly rotating black hole is favored ('faster is better'). We also find in the case of  $a=0.95$  that (i) the stagnation region is clearly found in the jet region, (ii) the ordered poloidal field lines are seen in the jet, (iii) the jet region is surrounded by a 'Wall-like' structure that has a higher pressure than the jet region and contains strong vertical magnetic fields, and (iv) the jet is initiated by outgoing Poynting flux from the outer horizon of the black hole (Blandford-Znajek effect). The bulk Lorentz factor of the jet is still of the order of unity. However, energy density of electro-magnetic fields dominates the one of rest-mass in the jet. It can be expected that a relativistic jet will be seen if we perform a simulation for a longer time scale (of the order of 10 – 100 sec).

**Key words:** gamma rays:bursts — black hole physics — relativity — supernovae: general — accretion, accretion disks

## 1. Introduction

It is still unknown how the central engine of Long Gamma-Ray Bursts (hereafter it is called as GRBs for simplicity) is working at the center of massive stars. In other words, we poorly know the engine that drives the most powerful explosion in the universe. Some of the supernovae that associate with GRBs were very energetic. Their energies were of the order of  $10^{52}$  ergs, which is  $\sim 10$  times larger than the ones of normal core-collapse supernovae. This fact strongly suggests that other engine from the one of normal core-collapse supernovae should be working at the center of the GRB's progenitors.

There are some possible scenarios to drive a GRB jet. One of the most promising scenarios is the collapsar scenario (Woosley 1993). In this study, we investigate the collapsar scenario. In the collapsar scenario, a black hole is formed as a result of gravitational collapse. Also, rotation of the progenitor plays an important role. Due to the rotation, an accretion disk is formed around the equatorial plane. After the formation of the accretion disk, there are several possible stories as below.

One is that a jet-induced explosion along the rotation axis may occur due to the heating through neutrino anti-neutrino pair annihilation that are emitted from the accretion disk (Woosley 1993; MacFadyen & Woosley 1999; Fryer & Mészáros 2000; Nagataki et al. 2003a; Nagataki et al. 2007; Sekiguchi and Shibata 2007; Barkov and Komissarov 2010; Harikae et al. 2010). This is an interesting possibility, although neutrino heating efficiency looks small (0.1 – 1%). A very careful treat-

ment of neutrino transfer with conserved-scheme of hydrodynamics will be necessary to prove that this effect is the key-process of GRB's engine.

Another is that a jet is driven by extracting rotational energies of the accretion disk with a help of magnetic fields that pierce the disk (Blandford-Payne effect: Blandford and Payne 1982). This scenario is also investigated by several authors (Proga et al. 2003; Proga and Begelman 2003; Mizuno et al. 2004a; Mizuno et al. 2004b; Proga 2005; Fujimoto et al. 2006; Nagataki et al. 2007; Suwa et al. 2007; Harikae et al. 2009). This is also a promising possibility. Further study will be necessary whether a relativistic jet will be launched by this mechanism.

Recently, the effect of extraction of rotation energy from the black hole through outgoing Poynting flux (Blandford-Znajek effect: Blandford and Znajek 1977) is investigated by using a General Relativistic Magneto-hydro Dynamics (GRMHD) code (Barkov and Komissarov 2008; Komissarov and Barkov 2009a; Nagataki 2009; Barkov and Komissarov 2010). Energy extraction from a rotating black hole is a general relativistic effect, so GRMHD code is necessary to investigate the effect. In Barkov and Komissarov (2008), they showed that a jet is launched by Blandford-Znajek effect using a Kerr black hole with Kerr parameter ( $a=0.9$ ) and a polytrope density profile for a massive star model. In their successive papers (Komissarov and Barkov (2009a), Barkov and Komissarov 2010), they also succeeded to launch a jet by Blandford-Znajek effect (Kerr Parameter was chosen to be 0.9 in Komissarov and Barkov 2009a, while 0.46 and 0.6 in Barkov and Komissarov 2010) using a polytrope density

profile for a massive star model. In Nagataki (2009), it was shown that a jet is launched by Blandford-Znajek effect (Kerr parameter was chosen to be 0.5) using a realistic progenitor model developed by Woosley and Heger (2006). In Nagataki (2009), it was pointed out that Blandford-Payne effect may be also working.

As stated above, in the previous papers, it was shown that a jet is successfully launched by Blandford-Znajek effect. However, there is no systematic study how the dynamics depends on the Kerr parameter. It is true that Komissarov and Barkov (2010) presented results for different Kerr parameters, but they also changed the amplitude of the initial magnetic fields. Also, no simulation has been reported for  $a = 0$ , that is, Schwarzschild black hole case. By performing a simulation for that case, we can clearly see how effectively the rotating black hole is working to drive the jet. In this study, we present 4 simulations for the same initial condition with Nagataki (2009), but with different Kerr parameters  $a = 0, 0.5, 0.9, 0.95$ . It is shown clearly that a more rapidly rotating black hole is driving a more energetic jet. Especially, in the case of the Schwarzschild case, no jet is found. That proves that the jet is really driven by the rotating black hole.

In section 2, method of calculation is explained. In section 3, initial condition is shown. Results are given in section 4. Discussion is presented in section 5. Conclusion is stated in section 6.

## 2. Method of Calculation

In this study, we use the GRMHD code developed in Nagataki (2009). Thus we briefly explain the method of calculation here, and please see Nagataki (2009) for details.

In Nagataki (2009), we have developed a two-dimensional GRMHD code following Gammie et al. (2003) and Noble et al. (2006). We have adopted a conservative, shock-capturing scheme with Harten, Lax, and van Leer (HLL) flux term (Harten et al. 1983) and flux-interpolated constrained transport technique (Tóth 2000). We use a third-order Total Variation Diminishing (TVD) Runge-Kutta method for evolution in time, while monotonized central slope-limited linear interpolation method is used for second-order accuracy in space (van Leer 1977). 2D scheme (2-dimensional Newton-Raphson method) is usually adopted for transforming conserved variables to primitive variables (Noble et al. 2006).

When we perform simulations of GRMHD, Modified Kerr-Schild coordinate is basically adopted with mass of the black hole ( $M$ ) fixed where the Kerr-Schild radius  $r$  is replaced by the logarithmic radial coordinate  $x_1 = \ln r$ . When we show the result, the coordinates are transferred from Modified Kerr-Schild coordinates to Kerr-Schild ones. In the following, we use  $G = M = c = 1$  unit.  $G$  is the gravitational constant,  $c$  is the speed of light, and  $M$  is the gravitational mass of the black hole at the center.

## 3. Initial Condition

The initial condition is also same with Nagataki (2009), but for different Kerr Parameters. Thus we explain it briefly here, and please see Nagataki (2009) for details.

The calculated region corresponds to a quarter of the meridian plane under the assumption of axisymmetry and equatorial symmetry. The spherical mesh with  $256(r) \times 128(\theta)$  grid points is used for all the computations. The radial grid is nonuniform, extending from  $r = 0.98r_+$  to  $3 \times 10^4$  ( $r_+ = 1 + \sqrt{1 - a^2}$  is the outer horizon, and  $3 \times 10^4$  corresponds to  $8.9 \times 10^9$  cm in cgs units) with uniform grids in the Modified Kerr-Schild coordinate.

We adopt the model 12TJ in Woosley and Heger (2006) (as for the progenitor evolution model, see e.g., Tutukov and Fedorova 2007). This model corresponds to a star that has  $12M_\odot$  initially with 1% of solar metallicity, and rotates rapidly and does not lose its angular momentum so much by adopting small mass loss rate. As a result, this star has a relatively large iron core of  $1.82M_\odot$ , and rotates rapidly at the final stage. We assume that the central part of the star has collapsed and formed a black hole of  $2M_\odot$ . Since  $M = 2M_\odot$ ,  $r = 1$  corresponds to  $2.95 \times 10^5$  cm. We also assume that the gravitational mass of the black hole is unchanged throughout the calculation. In Nagataki (2009), the Kerr parameter,  $a$ , was assumed to be 0.5, but in this study we perform simulations for  $a = 0, 0.5, 0.9, 0.95$ , respectively (we name them as Model A, B, C, D, respectively).

Since 1-D calculation is done for the model 12TJ, we can use the data directly for the physical quanta on the equatorial plane. As for the density, internal energy density, and radial velocity, we assume the structure of the star is spherically symmetric. We also set  $u^\theta = 0$  initially. As for  $u^\phi$ , we extrapolate its value such as  $u^\phi(r, \theta) = u^\phi(r, \pi/2) \times \sin \theta$ .

We assume the vector potential  $A_\phi \propto \max(\rho/\rho_{\max} - 0.2, 0) \sin^4 \theta$  where  $\rho_{\max}$  is the peak density in the progenitor (after extracting the central part of the progenitor that has collapsed and formed a black hole). The field is normalized so that the minimum value of  $p_{\text{gas}}/p_{\text{mag}} = 10^2$  where  $p_{\text{gas}}$  is the thermal pressure and  $p_{\text{mag}}$  is the magnetic pressure.

We use a simple equation of state  $p_{\text{gas}} = (\Gamma - 1)u$  where  $u$  is the internal energy density. We set  $\Gamma = 4/3$  so that the equation of state roughly represents radiation gas.

As for the boundary condition in the radial direction, we adopt the outflow boundary condition for the inner and outer boundaries. As for the boundary condition in the zenith angle direction, axis of symmetry boundary condition is adopted for the rotation axis, while the reflecting boundary condition is adopted for the equatorial plane. As for the magnetic fields, the equatorial symmetry boundary condition, in which the normal component is continuous and the tangential component is reflected, is adopted.

## 4. Results

In figure 1, contours of rest mass density in logarithmic scale for all models at the same time-slice  $t = 160000$  (that corresponds to 1.5760 sec) are shown. Cgs units are used for the rest mass density, while the length in the vertical/horizontal axes is written in  $G = M = c = 1$  unit.  $r = 1$  and 4000 corresponds to  $2.95 \times 10^5$  cm and  $1.18 \times 10^9$  cm, respectively. These results are projected on the  $(r \sin\theta, r \cos\theta)$ -plane. Upper left panel shows the state of Model A ( $a = 0$ ), upper right panel shows the one of Model B ( $a = 0.5$ ), lower left panel shows the one of Model C ( $a = 0.9$ ), and lower right panel shows the one of Model D ( $a = 0.95$ ). It is clearly shown that the rotating black hole drives the jet (the Schwarzschild black hole cannot drive a jet (Model A), while a more rapidly rotating black hole is driving a stronger jet).

From figure 2 to 6, we show the results for Model D at  $t = 160000$  (that corresponds to 1.5760 sec). The length in the vertical/horizontal axes is written in  $G = M = c = 1$  unit ( $r = 1, 20, 100$  correspond to  $2.95 \times 10^5$  cm,  $5.9 \times 10^6$  cm,  $2.95 \times 10^7$  cm, respectively).

In figure 2, color-contours of rest mass density in logarithmic scale (cgs units) with velocity fields (arrows) are shown. It is noted that stagnation region where the radial velocity becomes positive (outgoing) from negative (accreting) is seen around  $r = 15$  in the jet. In contrast, it is shown later (in figure 5) that outgoing Poynting flux is positive from the outer horizon.

In figure 3, color-contours of rest mass density in logarithmic scale (cgs units) with contours of the  $\phi$  component of the vector potential ( $A_\phi$ ) are shown. Level surfaces coincide with poloidal magnetic field lines, and field line density corresponds to poloidal field strength. Upper panel shows the central region ( $20 \times 20$ ), while lower panel shows the wider region ( $100 \times 100$ ). In the upper panel, the ordered poloidal field lines are seen in the jet. In the lower panel, a 'Wall-like' structure that contains vertical magnetic fields is seen.

In figure 4, contours of total pressure (sum of thermal and magnetic pressure) in logarithmic scale. Cgs units are used for the pressure contours are shown. It is clearly seen that the 'Wall-like' structure has high pressure: it is higher than the one in the jet region.

In figure 5, contours of outgoing Poynting flux ( $F_E$  in Eq.1) in logarithmic scale. It is noted that the total energy flux, which is the integrated outgoing Poynting flux over the zenith angle, can be written as

$$\dot{E} = 2\pi \int_0^\pi d\theta \sqrt{-g} (-T_{EM,t}^r) = 2\pi \int_0^\pi d\theta F_E, \quad (1)$$

where  $g$  and  $T_{EM,t}^r$  are determinant of the metric and  $(r,t)$  component of energy-momentum tensor of electromagnetic fields. The unit of the contours is  $10^{50}$  erg  $s^{-1}$   $sr^{-1}$ . Outer horizon is seen at the center ( $r_+ = 1.312$ ). It is clearly seen that outgoing Poynting flux is coming out from the outer horizon. This figure clearly shows that Blandford-Znajek process is working in this system. We could see also a powerful outgoing Poynting flux toward

the accretion disk. Partially this may be working for the variability of the mass accretion rate seen in Nagataki (2009).

In figure 6, contours of the electro-magnetic field energy flux per unit rest-mass flux are shown, which represent the bulk Lorentz factor of the inviscid fluid element when all of the electro-magnetic field energy are converted into kinetic energy (Nagataki 2009). Even though the bulk Lorentz factor of the jet is still low (of the order of unity), the terminal bulk Lorentz factor can be relativistic.

Finally, in figure 7, plots of the jet energy for all models at  $t = 160000$  are shown. The definition of the jet energy is:

$$E_{\text{Jet}} = 2 \times 2\pi \int_{r_+}^{\infty} dr \int_0^\theta d\theta \sqrt{-g} (T_t^t - \rho u^0 u_0), \quad (2)$$

where  $T_t^t$  is the  $(t,t)$  component of total energy-momentum tensor and integration is done only for the region where  $u^r$  (radial component of 4-velocity of fluid) is positive. It is noted that the contribution of the rest mass energy is subtracted. Factor 2 is coming from the symmetry of the system with respect to the equatorial plane. Blue curve represents the jet energy within the opening angle  $\theta = 5^\circ$ , while red curve represents the one within  $\theta = 10^\circ$ . The unit of vertical axis is  $10^{48}$  erg. It is clearly seen that a more rapidly rotating black hole is driving a stronger jet. The total energy of the jet for Model D ( $a = 0.95$ ) is as large as  $10^{50}$  erg. For comparison, the analytic curves of the BZ-flux formulation of Tchekhovskoy et al. (2010) for the case of monopole solution  $B = 5 \times 10^{14}$  G are shown by the red-dashed curve (until forth power of  $\Omega_H = a/2r_H$  where  $r_H$  is the horizon of the black hole). The analytic curve of the BZ-flux formulation of Tanabe and Nagataki (2008) for the case of  $B = 5 \times 10^{14}$  G is shown by the black-dashed curve (until forth power of  $a$ ). It is seen that the jet energy obtained in this study fits well with the previous analytical formulations.

## 5. Discussion

### 1. Whole Picture.

In section 4, we could see that a stronger jet is driven by a more rapidly rotating black hole. It is clear that the rotating black hole is driving the jet. In fact, no jet is seen for the case of Model A ( $a = 0$ ). On the other hand, the total energy of the jet for Model D ( $a = 0.95$ ) is as large as  $10^{50}$  erg. We showed some figures for Model D to understand the dynamics more clearly. We have found that (i) the stagnation region is seen around  $r = 15$  in the jet region, (ii) the ordered poloidal field lines are seen in the jet (that is consistent with other previous study on the jet formation from a torus (e.g. McKinney & Gammie 2004)), (iii) the jet region is surrounded by a 'Wall-like' structure that has a higher pressure than the jet region and contains strong vertical magnetic fields, and (iv) the jet is initiated by outgoing Poynting flux from the outer horizon. effect (Blandford-Znajek effect).

### 2. Wall-Like Structure.

We found the 'Wall-like' structure around the jet. It is

considered that the structure will depend on the initial angular momentum and density profile of the progenitor star and initial configuration and its strength of magnetic fields. We should investigate this feature by performing some simulations systematically as a next step. However, this Wall-like structure seems not to work so much for the formation and collimation of the jet, because the collimated jet has been launched already before the formation of the Wall-like structure.

### 3. Jet Energy.

It has been shown that the jet energy can be as large as  $10^{50}$  erg in 1.5 sec for Model D. Thus we expect that the energy of the jet can be  $\sim 10^{51}$  erg in 10 sec, and we can say that Blandford-Znajek mechanism is very promising to drive a GRB jet. On the other hand, for a slowly-rotating black hole case, the jet power looks too low, because the luminosity of a GRB jet ( $10^{51}$  erg  $s^{-1}$ ) is hard to explain. Thus it is concluded that a rapidly rotating black hole is favored ('faster is better'). This result is consistent with some previous test calculations (Tanabe and Nagataki 2008; Tchekhovskoy et al. 2010). Due to the limit of computational resources, we had to stop the simulation at  $t = 160000$  in this study. We are going to present a simulation that should last more than 10 sec in the near future.

### 4. Lorentz Factor.

It is found that the bulk Lorentz factor of the jet cannot be so high in this study (of the order of unity), although the electro-magnetic field energy flux is much greater than rest-mass flux in the jet, which was also seen in Nagataki (2009). We believe this jet has a good property, because the jet speed will become relativistic if the electro-magnetic field energy is converted to kinetic energy through the propagation. Also, we can be optimistic because the Wall-like structure was found in our simulations. It is pointed out that such a Wall is necessary to drive a relativistic jet in some papers (Komissarov et al. 2009b; Tchekhovskoy et al. 2010). Moreover, there have been many papers on the propagation of relativistic jet from a massive star (Aloy et al. 2000; Aloy et al. 2002; Zhang et al. 2003; Zhang et al. 2004; Mizuta et al. 2006; Mizuta and Aloy 2009; Morsony et al. 2007; Wang et al. 2008; Morsony et al. 2010; Mizuta et al. 2010; Nagakura et al. 2010) where the jet is driven by injecting energy from the inner boundary. Some of their results suggest that the bulk Lorentz factor of the jet will be increasing with time (e.g. Mizuta et al. 2010) because the material of the progenitor star is blown off and the jet region becomes 'cleaner' with time. Thus we expect that a relativistic jet will be seen if we perform a simulation for a longer time scale (of the order of 10 – 100 sec. see also Suwa and Ioka 2010).

### 5. Blandford-Payne Effect.

In this study, we showed that Blandford-Znajek effect is working. On the other hand, it was found that no jet was driven with a help of rotation of the accretion disk (Blandford-Payne effect) in Model A ( $a = 0$ ). Of course there is a possibility that the disk will drive a jet later. Also, the interaction between the rotating black hole and

the accretion disk may be important. That is, if the rotating black hole is connected with the accretion disk by magnetic fields and rotation power is conveyed to the disk, Blandford-Payne effect will become more effective. Further study will be necessary to conclude the necessity of Blandford-Payne effect to drive a GRB jet.

### 6. Microphysics.

In this study, microphysics such as neutrino physics and nuclear reaction is not included. The disk structure is deformed by neutrino cooling process (Popham et al. 1999; Nagataki and Kohri 2002; Nagataki et al. 2003a; Nagataki et al. 2007; López-Cámara et al. 2010; Linder et al. 2010; Taylor et al. 2010; Sekiguchi and Shibata 2010). Nucleosynthesis study provides us with an opportunity to compare the simulations with observations of supernova ejecta and supernova remnants (Nagataki et al. 1997; Nagataki et al. 1998a; Nagataki et al. 1998b; Nagataki 2000; Maeda et al. 2002; Nagataki et al. 2003b; Takiwaki et al. 2004; Nagataki et al. 2006; Maeda et al. 2007; Tominaga 2009; Ramirez-Ruiz and MacFadyen 2010; Milosavljevic et al. 2010). We are planning to include these microphysics as a next step.

### 7. 3D Simulation.

We showed our results of two-dimensional (2D) simulations in this study. It will be important to compare the 2D simulations with 3D ones. In 3D simulations, hydrodynamic instability in the azimuthal direction will be seen (Nagakura & Yamada 2008; Nagakura & Yamada 2009; Mckinney & Blandford 2009).

## 6. Conclusion

We have performed 4 simulations of collapsars with different Kerr parameters  $a = 0, 0.5, 0.9, 0.95$ . It is clearly shown that a more rapidly rotating black hole is driving a more energetic jet. No jet is seen for the case of Model A ( $a = 0$ ), while the total energy of the jet for Model D ( $a = 0.95$ ) is as large as  $10^{50}$  erg. We expect that the energy of the jet can be  $\sim 10^{51}$  erg in 10 sec for Model D. In order to explain the high luminosity of a GRB, it is concluded that 'faster is better'.

We have found in Model D that (i) the stagnation region is seen around  $r = 15$  in the jet region, (ii) the ordered poloidal field lines are seen in the jet, (iii) the jet region is surrounded by the 'Wall-like' structure that has a higher pressure than the jet region and contains strong vertical magnetic fields, and (iv) the jet is initiated by outgoing Poynting flux from the outer horizon (Blandford-Znajek effect).

As for the bulk Lorentz factor, it is still not so high in this study (of the order of unity), although energy density of electro-magnetic field dominates the one of rest-mass in the jet. We expect that a relativistic jet will be seen if we perform a simulation for a longer time scale (of the order of 10 – 100 sec).

This research was supported by Grant-in-Aid for Scientific Research on Priority Areas No. 19047004 and Scientific Research on Innovative Areas No. 21105509

by Ministry of Education, Culture, Sports, Science and Technology (MEXT), Grant-in-Aid for Scientific Research (S) No. 19104006 and Scientific Research (C) No. 21540404 by Japan Society for the Promotion of Science (JSPS), and Grant-in-Aid for the Global COE Program "The Next Generation of Physics, Spun from Universality and Emergence" from MEXT of Japan. The computation was carried out on NEC SX-8 at Yukawa Institute for Theoretical Physics (YITP) in Kyoto University and Cray XT4 at Center for Computational Astrophysics (CfCA) in National Astronomical Observatory of Japan (NAOJ).

## References

- Aloy, M.A., Müller, E., Ibáñez, J.M., Mrtí, J.M., MacFadyen, A.I. 2000, ApJ, 531, L119
- Aloy, M.A., Ibáñez, J.M., Miralles, J.-A., Urpin, V. 2002, A&A, 396, 693
- Barkov, M., Komissarov, S.S. 2008, MNRAS, 385, L28
- Barkov, M., Komissarov, S.S. 2010, MNRAS, 401, 1644
- Blandford, R.D., Znajek, R.L. 1977, MNRAS, 179, 433
- Blandford, R.D., Payne, D.G. 1982, MNRAS, 199, 883
- Fryer, C., Mészáros, P. 2000, ApJ, 588, L25
- Fujimoto, S., et al. 2006, ApJ, 644, 1040
- Gammie, C.F., McKinney, J.C., Tóth, G. 2003, ApJ, 589, 444
- Harikae, S., Takiwaki, T., Kotake, K. 2009, ApJ, 704, 354
- Harikae, S., Kotake, K., Takiwaki, T., Sekiguchi, Y. 2010, ApJ, 720, 614
- Harten, A., Lax, P.D., van Lerr, B. 1983, SIAM Rev. 25, 35
- Komissarov, S.S., Barkov, M. 2009a, MNRAS, 397, 1153
- Komissarov, S.S., Vlahakis, N., Königl, A., Barkov, M. 2009b, MNRAS, 394, 1182
- Linder, C.C., Milosavljević, M., Couch, S.M., Kumar, P. 2010, ApJ, 713, 800
- López-Cámara, D., Lee, W.H., Ramirez-Ruiz, E. 2010, ApJ, 716, 1308
- MacFadyen, A.I., Woosley, S.E. 1999, ApJ, 524, 262
- Maeda, K., et al. 2002, ApJ, 565, 405
- Maeda, K., et al. 2007, ApJ, 658, 5
- McKinney, J.C., Gammie, C.F. 2004, ApJ, 611, 977
- McKinney, J.C., Blandford, R. 2008, MNRAS, 394, 126
- Milosavljevic, M., Linder, C.C., Shen, R., Kumar, P. 2010, arXiv:1007.0763
- Mizuno, Y., Yamada, S., Koide, S., Shibata, K. 2004a, ApJ, 606, 395
- Mizuno, Y., Yamada, S., Koide, S., Shibata, K. 2004b, ApJ, 615, 389
- Mizuta, A., Yamasaki, T., Nagataki, S., Mineshige, S. 2006, ApJ, 651, 960
- Mizuta, A., Aloy, M.A. 2009, ApJ, 699, 1261
- Mizuta, A., Nagataki, S., Aoi, J. 2010, arXiv:1006.2440
- Morsony, B.J., Lazzati, D., Begelman, M.C. 2007, ApJ, 665, 569
- Morsony, B.J., Lazzati, D., Begelman, M.C. 2010, ApJ, 723, 267
- Nagakura, H., Yamada, S. 2008, ApJ, 689, 391
- Nagakura, H., Yamada, S. 2009, ApJ, 696, 2026
- Nagakura, H., Ito, H., Kiuchi, K., Yamada, S. 2009, arXiv:1009.2326
- Nagataki, S., Hashimoto, M., Sato, K., Yamada, S. 1997, ApJ, 486, 1026
- Nagataki, S., Shimizu, T., Sato, K. 1998a, ApJ, 495, 413
- Nagataki, S., Hashimoto, M., Sato, K., Yamada, S., Mochizuki, Y.S. 1998b, ApJ, 492, L45
- Nagataki, S. 2000, ApJS, 127, 141
- Nagataki, S., Kohri, K. 2002, PThPh, 108, 789
- Nagataki, S., Kohri, K., Ando, S., Sato, K. 2003a, Aph, 18, 551
- Nagataki, S., Mizuta, A., Yamada, S., Takabe, H., Sato, K. 2003b, ApJ, 596, 401
- Nagataki, S., Mizuta, A., Sato, K. 2006, ApJ, 647, 1255
- Nagataki, S., Takahashi, R., Mizuta, A., Takiwaki, T. 2007, ApJ, 659, 512
- Nagataki, S. 2009, ApJ, 704, 937
- Noble, S.C., Gammie, C.F., McKinney, J.C., Del Zanna, L. 2006, ApJ, 641, 626
- Popham, R., Woosley, S.E., Fryer, C. 1999, ApJ, 518, 356
- Proga, D., MacFadyen, A.I., Armitage, P.J., Begelman, M.C. 2003, ApJ, 599, L5
- Proga, D., Begelman, M.C. 2003, ApJ, 582, 69
- Proga, D. 2005, ApJ, 629, 397
- Ramirez-Ruiz, E., MacFadyen, A.I. 2010, ApJ, 716, 1028
- Sekiguchi, Y., Shibata, M. 2010, arXiv:1009.5303
- Sekiguchi, Y., Shibata, M. 2007, PThPh, 124, 331
- Suwa, Y., Takiwaki, T., Kotake, K., Sato, K. 2007, PASJ, 59, 771
- Suwa, Y., Ioka, K. 2010, arXiv:1009.6001
- Takiwaki, T., Kotake, K., Nagataki, S., Sato, K. 2004, ApJ, 616, 1086
- Tanabe, K., Nagataki, S. 2008, PRD, 78, 024004
- Taylor, P.A., Miller, J.C., Podsiadlowski, Ph. 2010, MNRAS.tmp.1601
- Tchekhovskoy, A., Narayan, R., McKinney, J.C. 2010, ApJ, 711, 50
- Tominaga, N. 2009, ApJ, 690, 526
- Tóth, J. 2000, Compt. Phys. 161, 605
- Tutukov, A.V., Fedorova, A.V. 2007, Astronomy Reports, 51, 291
- van Leer, B.J. 1977, J. Compt. Phys. 23, 276
- Wang, P., Abel, T., Zhang, W. 2008, ApJ, 176, 467
- Woosley, S.E. 1993, ApJ, 405, 273
- Zhang, W., Woosley, S.E., MacFadyen, A.I. 2003, ApJ, 586, 356
- Zhang, W., Woosley, S.E., Heger, A. 2004, ApJ, 608, 365

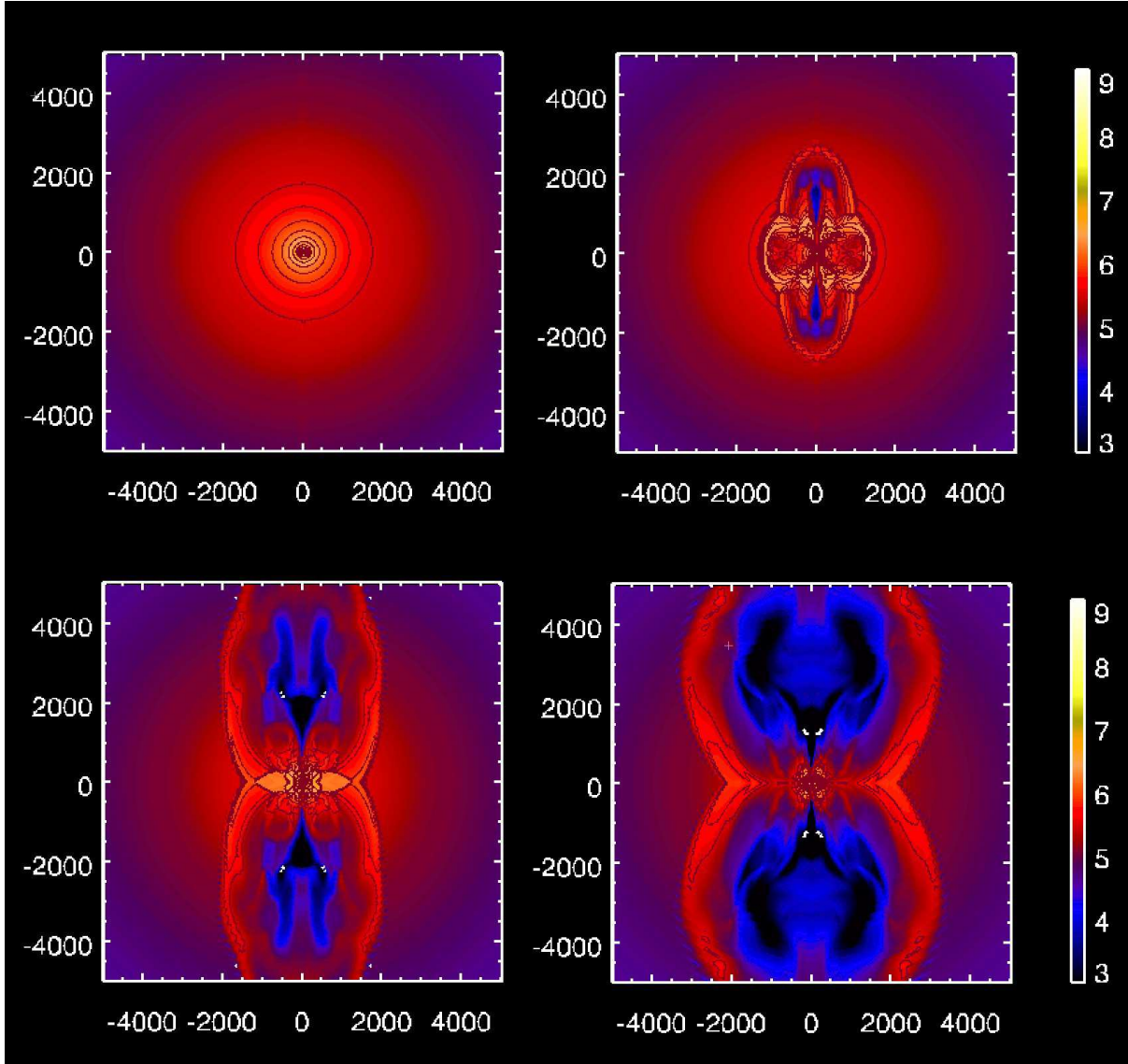


**Fig. 1.** Contours of rest mass density in logarithmic scale for all models at the same time-slice  $t = 160000$  (that corresponds to 1.5760 sec). Cgs units are used for the rest mass density, while the length in the vertical/horizontal axes is written in  $G = M = c = 1$  unit.  $r = 1$  and 4000 corresponds to  $2.95 \times 10^5$  cm and  $1.18 \times 10^9$  cm, respectively. These results are projected on the  $(r \sin \theta, r \cos \theta)$ -plane. Upper left panel shows the state of Model A ( $a = 0$ ), upper right panel shows the one of Model B ( $a = 0.5$ ), lower left panel shows the one of Model C ( $a = 0.9$ ), and lower right panel shows the one of Model D ( $a = 0.95$ ).

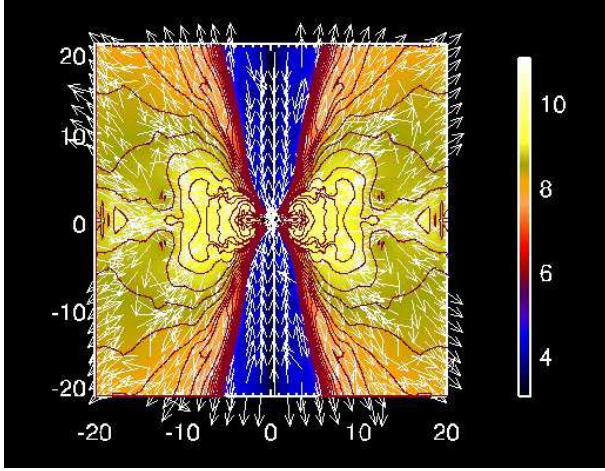


**Fig. 2.** Same with Figure 1, but for Model D ( $a = 0.95$ ) with velocity fields.  $r = 20$  corresponds to  $5.9 \times 10^6$  cm. Arrows represent the velocity fields ( $u^r, u^\theta$ ).

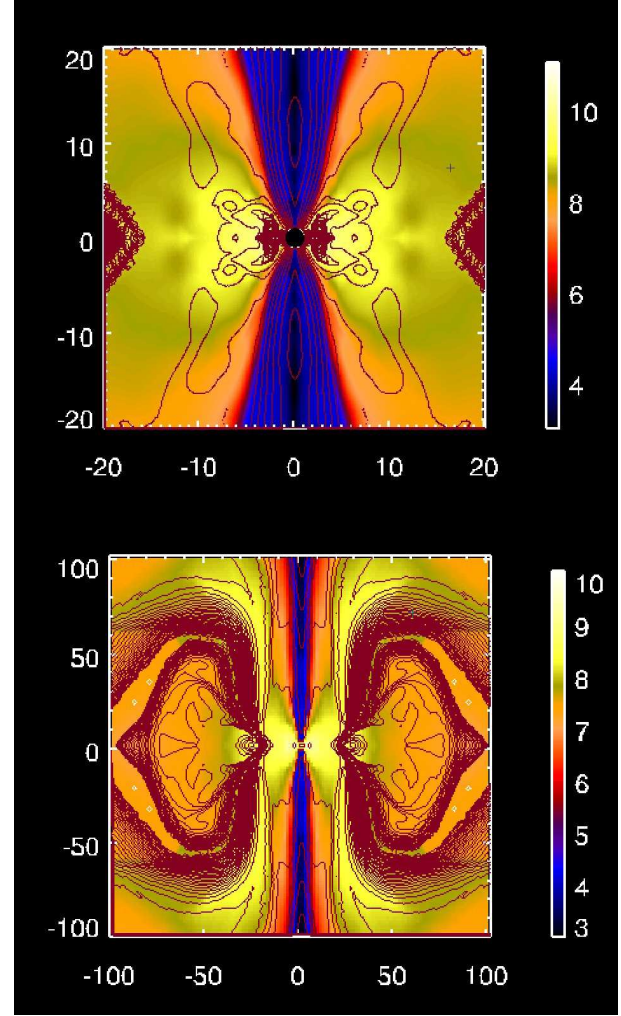


**Fig. 3.** Same with Figure 1, but for Model D ( $a = 0.95$ ) with line-contours of the  $\phi$  component of the vector potential ( $A_\phi$ ). Upper panel shows the central region ( $20 \times 20$  in  $G = M = c = 1$  unit), while lower panel shows the wider region ( $100 \times 100$ ).  $r = 100$  corresponds to  $2.95 \times 10^7$  cm.

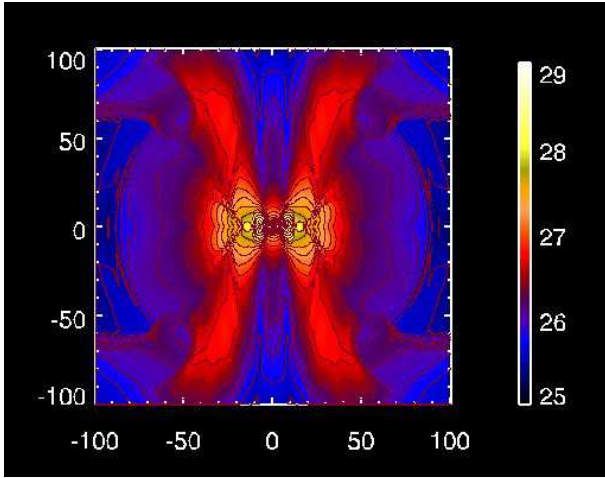


**Fig. 4.** Contours of total pressure (sum of thermal and magnetic pressure) in logarithmic scale at  $t = 160000$  (that corresponds to 1.5760 sec) for Model D ( $a = 0.95$ ). Cgs units are used for the pressure contours, while the length in the vertical/horizontal axes is written in  $G = M = c = 1$  unit.  $r = 100$  corresponds to  $2.95 \times 10^7$  cm.

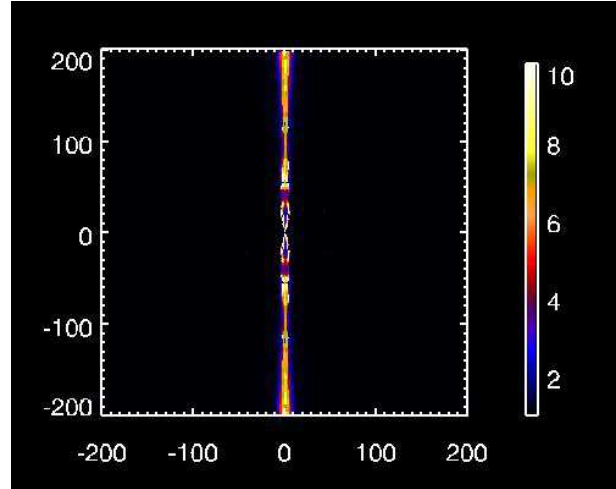


**Fig. 6.** Contours of the energy flux per unit rest-mass flux for Model D ( $a = 0.95$ ) at  $t = 160000$ . The contours represent the bulk Lorentz factor of the inviscid fluid element when all of the internal and magnetic energy are converted into kinetic energy.

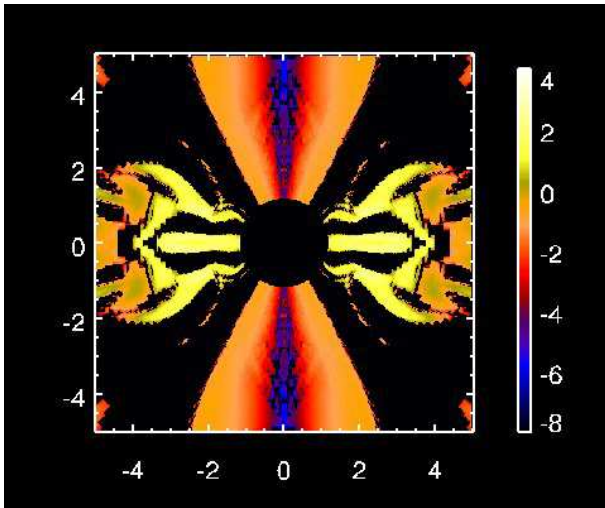


**Fig. 5.** Contours of outgoing Poynting flux in logarithmic scale at  $t = 160000$  (that corresponds to 1.5760 sec) for Model D ( $a = 0.95$ ). The unit of the contours is  $10^{50}$  erg  $s^{-1}$   $sr^{-1}$  (see text for the definition in detail), while the length in the vertical/horizontal axes is written in  $G = M = c = 1$  unit.  $r = 1$  corresponds to  $2.95 \times 10^5$  cm. Outer horizon is seen at the center ( $r_+ = 1.312$ ).

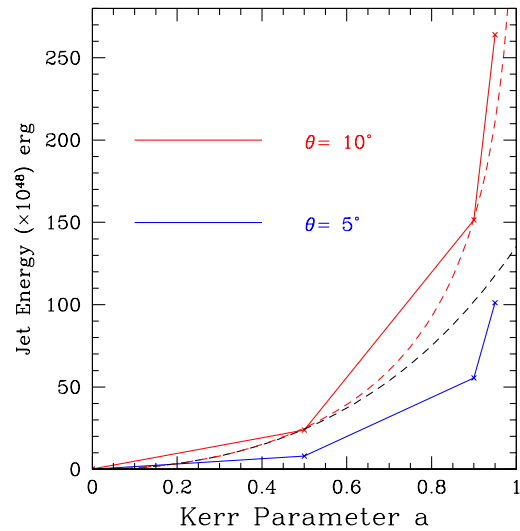


**Fig. 7.** Plots of the jet energy (see text for the definition in detail) for all models at  $t = 160000$  (that corresponds to 1.5760 sec). The unit of vertical axis is  $10^{48}$  erg. Blue curve represents the jet energy within the opening angle  $\theta = 5^\circ$ , while red curve represents the one within  $\theta = 10^\circ$ . The analytic curves of the BZ-flux formulation of Tchekhovskoy et al. (2010) for the case of monopole solution with  $B = 5 \times 10^{14}$  G are shown by the red-dashed curve (forth power of  $\Omega_H$ ). The analytic curve of the BZ-flux formulation of Tanabe and Nagataki (2008) for the case of monopole solution with  $B = 5 \times 10^{14}$  G is shown by the black-dashed curve (until forth power of  $a$ ).